

Atmospheric Science of Humid Areas: *Why Are Humid Areas Humid?*

Sumant Nigam

Department of Atmospheric & Oceanic Science, and the
Earth System Science Interdisciplinary Center
3419 Computer & Space Science Bldg. (224), 4254 Stadium Drive
University of Maryland, College Park, MD 20742
Email: nigam@umd.edu

Revised 31 May 2016

9th Biennial Rosenberg International Forum on Water Policy: *Managing Water and Biodiversity
in Humid Area*; Panama City, Panama; 25-28 January 2016

Abstract

The paper reviews the large-scale distribution of seasonal precipitation in the tropical and extratropical regions, focusing on the organizing dynamical and thermodynamical principles. It begins with a brief discussion on the existence of the Tropics and the unique seasonal variability within the Tropics of Cancer and Capricorn from the Sun being overhead twice each year.

Sea-surface temperature (SST) in the largely ocean-covered Tropics exerts a profound influence on the tropical and extratropical climate but, interestingly, its distribution is determined not just by the incident solar radiation – attesting to the importance of atmospheric and oceanic circulations, and clouds and convection, i.e., to complex feedbacks in the climate system.

The humidity in the Tropics is largely controlled by the surface temperature of the underlying oceans. The tropical troposphere holds about a week's rainfall in vapor form, called precipitable water. However, more than half of the moisture for tropical rainfall is imported from the subtropics – the oceanic deserts – via the low-level atmospheric circulation. Oceanic deserts are the low rainfall–clear sky regions of high surface salinity. Interestingly, the Atlantic is saltier than the Pacific, for reasons related to atmospheric moisture transports and the Isthmus of Panama!

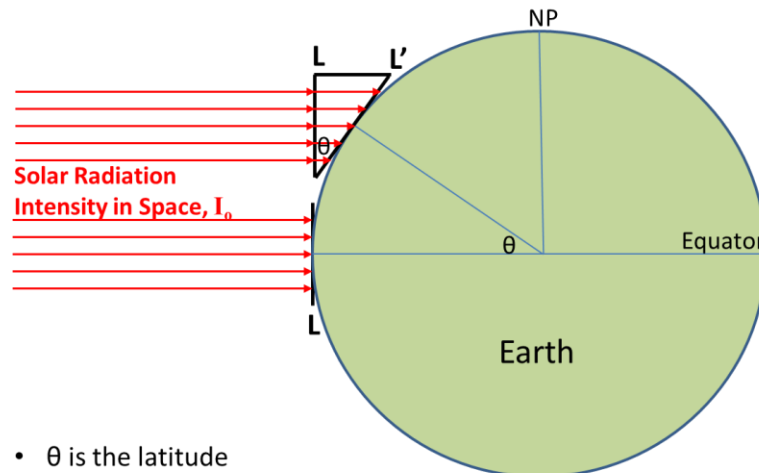
Transportation of moisture is a key element of the atmospheric water cycle. The regional transports can be highly organized in structure and phenomenal in volume, surpassing the flow of major rivers! The atmospheric water-cycle over the central equatorial Pacific – a region of high precipitation – will be discussed.

Finally, the substantial declining trends in summer precipitation over the Indo-Gangetic Plain and the lowlands/plains eastward of the Tibetan Plateau (home to 2 billion people) since the mid-20th century are analyzed for cause: Anthropogenic change or multidecadal natural variability?

1. The Origin of the Tropics

Humid areas commonly refer to the Tropics. The vast Earth-Sun distance – about 12,000 times the Earth’s diameter – allows solar radiation incident on the relatively small Earth (diameter one-hundredth of the Sun) to be treated as a parallel beam (Fig. 1). The solar radiation incident normal to the earth’s surface, the solar intensity $I(\theta)$, decreases with latitude (θ) as the cosine of θ , as indicated in Figure 1. As a result, the Equator (EQ) and neighboring latitudes receive much more solar energy than latitudes in the vicinity of the North Pole (NP). Of course, not all of the energy incident at the top of the atmosphere reaches the earth’s ocean-land surface. Some of it is absorbed in the atmosphere and some of it is reflected back to space. This attenuation notwithstanding, more solar energy arrives at the ocean-land surface in the equatorial and neighboring latitudes, generating the warm tropical climates.

The Origin of the Tropics: Earth-Sun Geometry



- θ is the latitude
- L and L' are the distance over which a given amount of solar energy is spread at the Equator and at latitude θ , respectively
- $L' = L/\cos(\theta)$, i.e., L' is always $\geq L$, as seen in the figure
- *Solar Intensity* $I(\theta)$ is solar energy per unit area (or linear distance in this schematic): $I(\theta) = I_0 \cos(\theta)$; $\cos(\text{EQ}) = 1.0$ and $\cos(\text{NP}) = 0.0$
- Intensity is thus largest at the Equator – ***The Origin of the Tropics***

Figure 1: Schematic view of the incidence of solar radiation on the Earth’s spherical surface. Note, the figure does not depict the tilt of the Earth’s rotational axis.

2. Annual Solar Radiation

The solar (shortwave) radiation incident at the top of the atmosphere (TOA), i.e., before atmospheric absorption and reflection, is displayed in Figure 2. The *annual-average* of the *daily-mean* incident energy is shown; the profound diurnal (day and night) and seasonal variations (e.g., North Pole dark in boreal winter) are averaged here. The top panel shows the TOA downward solar flux; not surprisingly, the field is longitudinally uniform. The equator-to-midlatitude (e.g., 45°N) drop-off is large, in excess of 100 W/m², or 25% of the equatorial value.

The downward solar flux at the earth's surface (middle panel) is significantly attenuated from clear-sky reflection (~27 W/m²), atmospheric absorption (~75 W/m²), and cloud reflection (~45 W/m²); the number in parentheses are approximate global averages. This attenuation results in

the central equatorial Pacific receiving ~250 W/m², or about 150 W/m² less than its TOA input. Some of the energy reaching the ocean-land surface is reflected back (~25 W/m²), for example, by snow (in polar regions) and the shiny ocean surface (in the Tropics), leaving a lesser amount available for absorption at the ocean-land surface, as shown in the bottom panel.

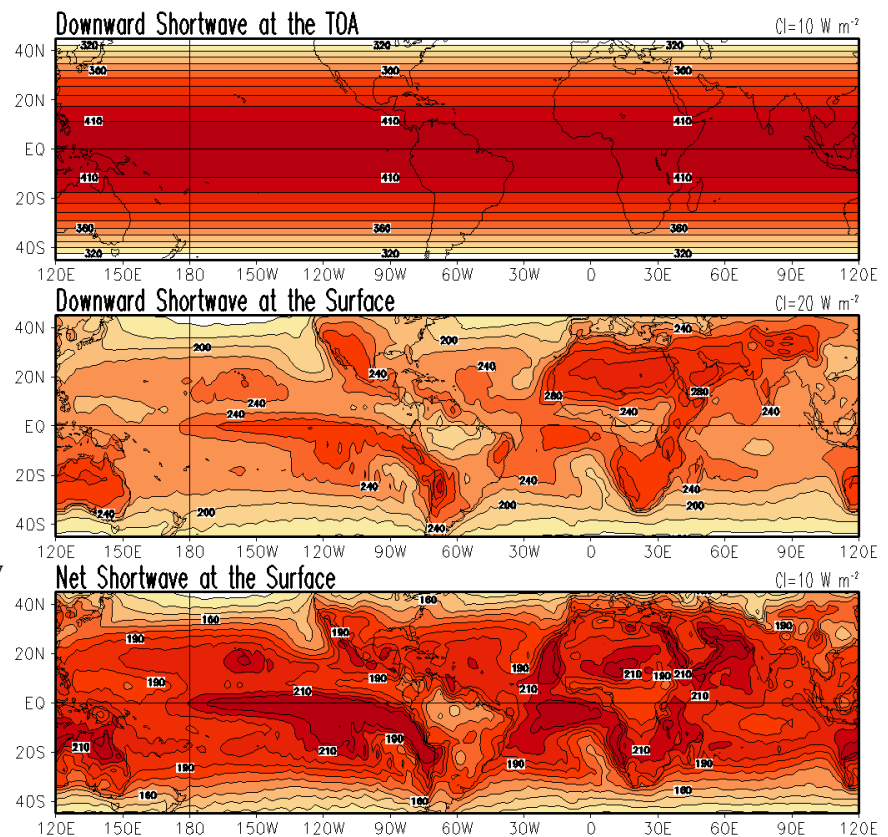


Figure 2: Annual-average of daily-mean solar radiation during 1979-2014: Downward flux at TOA (top); at surface (middle); and the net surface flux (downward minus reflected); all from NCEP Reanalysis (Kalnay et al. 1996).

3. Annual and Semi-Annual Variability in the Tropics

The seasonal variation in the daily-averaged solar radiation at the TOA is shown in Figure 3. The variation results primarily from the tilt of the earth's rotational axis with respect to the orbital plane – currently 23.4° -- and to a lesser extent from the ellipticity of the orbit (currently 0.017). The seasonal variability consists of a pronounced annual variations in the extratropics (i.e., north of the Tropic of Cancer in Northern Hemisphere, and south of the Tropic of Capricorn in Southern Hemisphere); for example, at 45°N (dashed red line), the incident flux is maximum at the summer solstice (SS) and minimum at the winter one (WS). These annual variations are manifest also at the surface and commonly appreciated. Within the Tropics however, the Sun is overhead twice each year – at the vernal and autumnal equinox (VE and AE) – leading to semi-annual variability at the Equator and vicinity, as evident from tracking of radiation along the solid line in the figure. Is semi-annual variability also manifest at the surface within the Tropics?

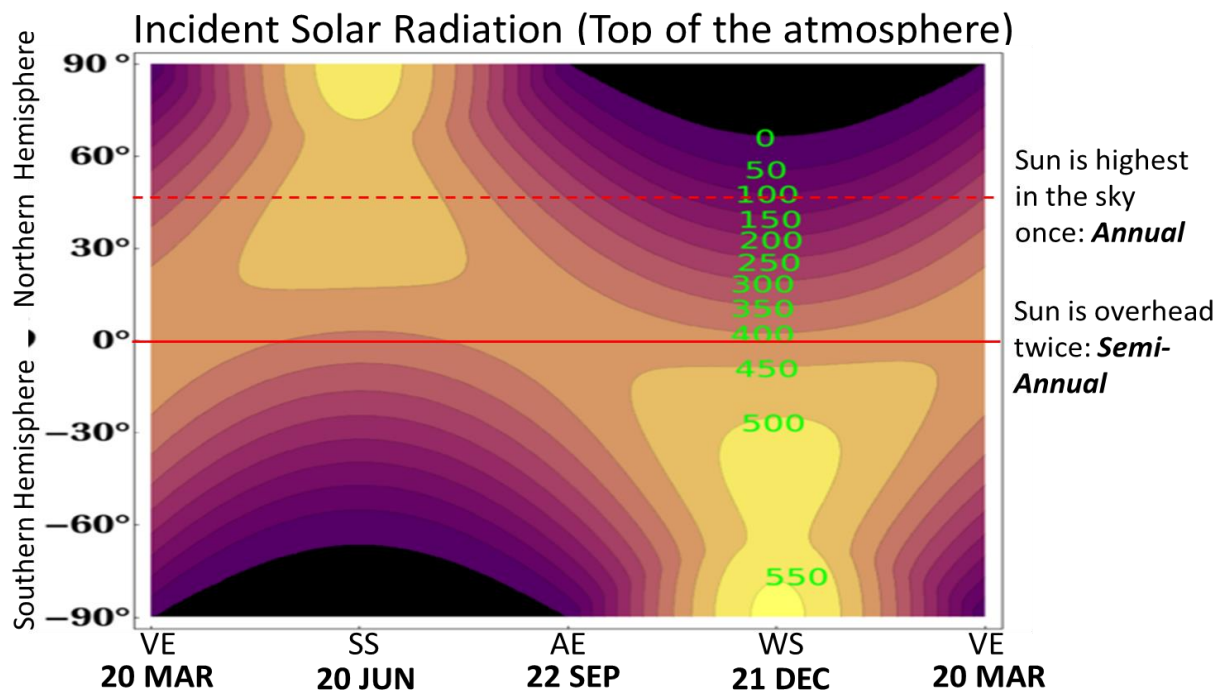


Figure 3: Daily-averaged solar radiation incident on the top of the atmosphere, in W/m^2 . VE and AE are vernal and autumnal equinox, and SS and WS are summer and winter solstices. (Available from <https://commons.wikimedia.org/wiki/File:InsolationTopOfAtmosphere.png>)

4. The Influential Sea Surface Temperature

The annual-mean sea surface temperature (SST) is shown in Figure 4. The SST distribution is determined from both thermodynamical and dynamical processes: The net surface shortwave flux (Fig. 2, bottom), the net surface longwave flux (not shown), and the sensible and latent heat fluxes (not shown) are the influential (and SST-influenced) thermodynamical processes, while equatorial and coastal upwelling, vertical mixing in the upper-ocean, and entrainment of thermocline water are the ocean dynamical processes influencing SST. These processes and their feedbacks notwithstanding, the SSTs exhibit an overall decline with increasing latitude, broadly

consistent with the latitudinal drop-off of the net surface shortwave flux (Fig. 2, bottom). That the latter is not the sole arbiter of SSTs is evident from the differences in longitudinal structure, e.g., the net surface shortwave flux is largest over the eastern tropical basins but SSTs are warmest in the western basins (Fig. 4, top panel) – the western warm pools.

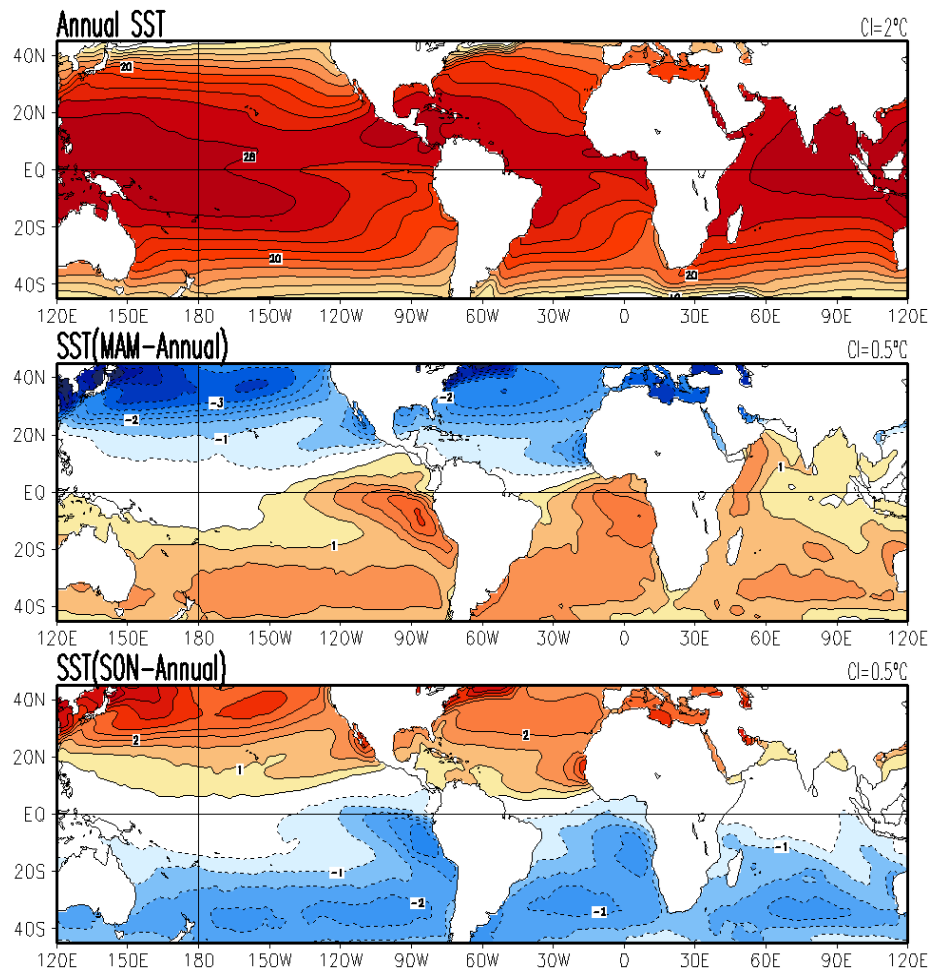


Figure 4: Sea surface temperature (SST) for the 1979-2014 period. Annual-average (top); March-May departure from annual-mean (middle); and the September-November departure (bottom). Data is from UK Met Office (HadISST 1.1; Rayner et al. 2003).

The seasonal departure of SSTs from their annual-mean value is shown during March-May (Fig. 4, middle) and September-October (Fig. 4, bottom), i.e., in periods immediately following the vernal and autumnal equinox. Although the Sun is overhead at the Equator at both these times, the two SSTs fields are very different: Warm SSTs in the eastern tropical Pacific and Atlantic in March-May, and cold ones there in September-November. The origin of this counterintuitive (and annual) SST response in the face of semi-annual solar forcing at the Equator (cf. Fig. 3) resides in the coupled ocean-atmosphere-land interactions instigated by the orientation of the coastlines, especially the continental overhang northward of the equator (e.g., Philander and Chao 1991; Mitchell and Wallace 1992; Nigam and Chao 1996), to which Panama contributes.

The departure of SST from its seasonal rhythm – for example, El Nino/La Nina variations in the central-eastern tropical Pacific on interannual timescales, and Pacific Decadal Oscillation in the tropical-extratropical basin (Mantua et al. 1997) – exert profound and far-reaching influence on regional hydroclimates (e.g., Deser et al. 2012), but these not of immediate interest here.

5. Humidity in the Tropics

The global Tropics, the region between the Tropic of Cancer and Capricorn, are for most part, ocean covered. The abundance of water and warm SSTs in the Tropics make the region very humid. Specific Humidity (SH) – the mass of water vapor divided by the mass of moist air in any given volume – is highest in the Tropics, as shown in Figure 5 (top). The annual-mean surface SH pattern (Fig. 5, top) has striking resemblance to the annual-mean SST pattern (Fig. 4, top), indicating SST control. Another humidity measure is Relative Humidity (RH), which measures the moistness of air relative to its maximum moisture-carrying capacity (i.e., saturated

state), in percentage. High RH reduces scope for further evaporation (e.g., of sweat), and is often the preferred metric for monitoring human comfort in the hot, humid environments. Annual-mean surface RH is shown in Figure 5 (middle), and vast stretches of the Tropics have RH greater than 80%. Although SH is higher over the warmer western tropical basins, RH is higher

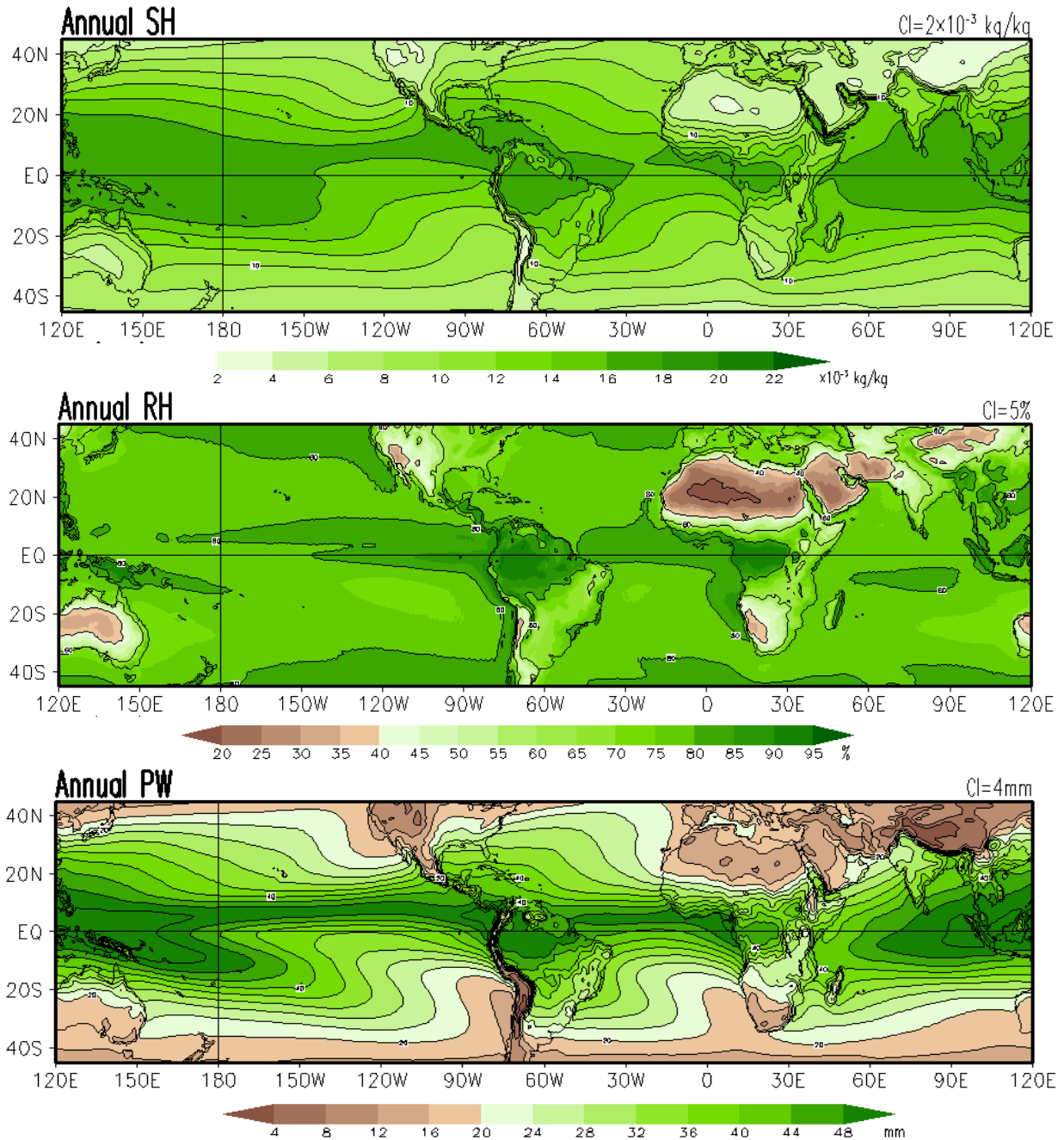


Figure 5: Annual-mean *surface* specific humidity (SH, top), *surface* relative humidity (RH, middle), and precipitable water (PW) during 1979-2014, from the European Centre for Medium Range Weather Forecast’s ERA Interim Reanalysis (Dee et al. 2011). Units: Kg of water per Kg of moist air (top), % (middle), mm of water (bottom).

over the eastern basins because these basin sectors lie under subsiding air (i.e., the descending branch of the Walker Circulation), which keeps the atmospheric boundary layer well-mixed. The bottom panel in Figure 5 shows precipitable water (PW), or the height of the water column (in millimeters) obtained by condensing all the water vapor contained in an atmospheric column stretching from the ocean-land surface to the tropical tropopause (located at ~15 Km height). PW values over the western Pacific warm pool often exceed 50 mm. As shown later, the precipitation rate here is ~ 7 mm/day, i.e., the tropical atmosphere holds about a week's rainfall in vapor form. The holding capacity is similar for the central Great Plains, where PW ~ 16-20 mm, and the precipitation rate 2-3 mm/day.

6. Precipitation in the Tropics

The element of the atmospheric water cycle that nourishes life on earth – precipitation – is shown in Figure 6. The precipitation, arriving primarily in liquid form in the Tropics and measured in millimeters of water per day, is not homogeneously distributed. It exhibits several coherent features the most prominent of which is the Inter-Tropical Convergence Zone (ITCZ) – a band of heavy precipitation extending across the ocean basins slightly northward of the Equator. The ITCZ is robust during July (Fig. 6, bottom), i.e., in boreal summer when it connects with the peak rainfall over the tropical NH landmasses (Maritime Continent to the west, Central America and northern South America, Central Africa including Sahel, and South Asia). Typical rainfall rates in the ITCZ are ~7 mm/day in January and ~10 mm/day in July. The summer monsoon rainfall over eastern India and Bangladesh is also ~10 mm/day, as also over Panama. Another coherent feature of precipitation distribution in the Tropics is the band of heavy precipitation emanating from the western tropical Pacific (the warm pool) and extending

southeastward into the SH subtropics. This feature, referred as the South Pacific Convergence Zone (SPCZ), is robust in the SH summer (i.e., January).

Also noteworthy in Figure 6 are the large unshaded (i.e., near-zero precipitation) regions on either side of the ITCZ in the central and eastern basins, especially during boreal spring and summer. These ‘oceanic deserts’ – devoid of clouds and rainfall – are clear-sky regions where solar energy arrives at the ocean surface with minimal attenuation, fueling evaporation. The evaporated moisture is carried great distances by the near-surface circulation in each hemisphere, especially towards the Equator where it converges in the core region of the ITCZ (e.g., Fig. 6, bottom). The inter-hemispheric convergence of the moisture-rich air leads to its ascent, and thus condensation and heavy rainfall. In short, moisture transports plays a critical role in the organization of precipitation, especially its coherent features. The near-surface circulation, in turn, is influenced by the latent heat released during precipitation (i.e., during the vapor-to-liquid phase transition) especially in the western-central basins where the ascent is deep into the troposphere. Such feedbacks can lead to potential self-organization of the SST-circulation-precipitation distributions.

Moisture transports also play an important role in shaping the precipitation distribution over continents. The coherent low-level (925 hPa) flow into the Caribbean Islands from the Atlantic and the onshore flow from the Gulf of Mexico into the southern-central Great Plains in July (Fig. 6, bottom) provide significant component of moisture for continental rainfall; the first flow feature is called the Caribbean Low Level Jet (e.g., Munoz et al. 2008) while the latter one is referred as the Great Plains Low-Level Jet (GPLLJ; e.g., Weaver and Nigam 2008). Low-level jets carry copious amounts of water, e.g., northward transport of moisture by the GPLLJ (whose core is at a height of ~ 1 Km above ground) is approximately three times the discharge of the

Mississippi flowing underneath! The low-level jets have, of course, long been appreciated in context of the summer monsoon over the Indian subcontinent, where the bulk of moisture from

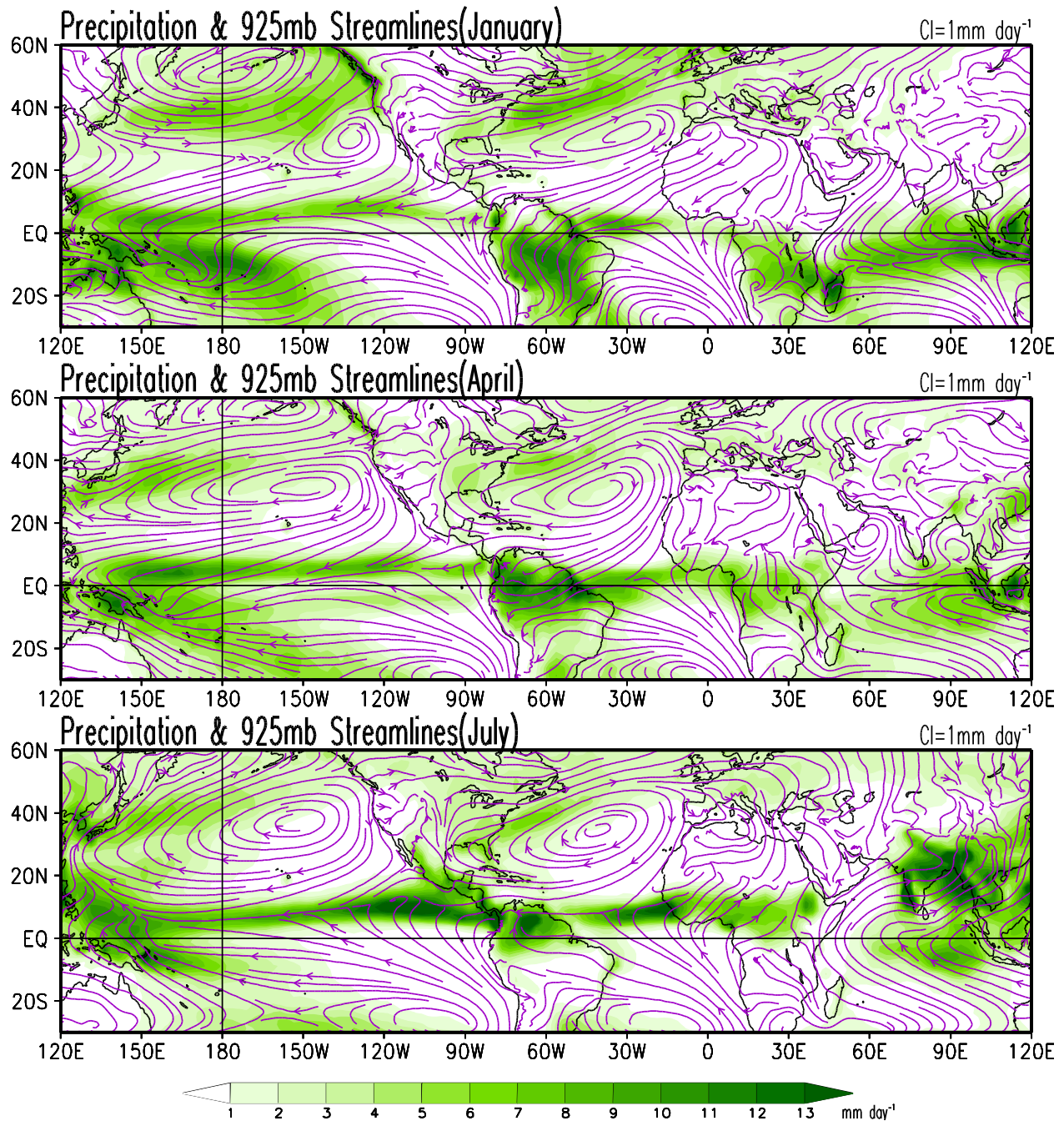


Figure 6: Climatological precipitation (shaded, in mm/day) and the horizontal wind direction (represented by streamlines) at a height of ~1 Km above the surface (more precisely, at the 925 hPa pressure surface) in January (top), April (middle), and July (bottom). Precipitation is from the Global Precipitation Climatological Project (GPCP V2.2; Adler et al. 2003), a blended satellite-rain-gauge based estimate, while streamlines are from the ERA-Interim atmospheric reanalysis. Climatology is based on the 1979-2014 period – the satellite-era.

the Indian Ocean arrives via the cross-equatorial Somali Low Level Jet (also discernible in Fig. 6, bottom panel).

The ascending and descending regions, and thus precipitation distribution, in the midlatitudes are strongly shaped by dynamical considerations, e.g., vorticity dynamics induces descending motions over the eastern flank of the expansive clockwise circulation pattern over the extratropical Pacific basin in July (Fig. 6, bottom). Dynamically induced descent will inhibit precipitation; for this reason, California exhibits a sunny-dry (i.e., Mediterranean-type) summer climate. Eastern Mediterranean is sunny and dry in summer for the same reasons – being in the vicinity of the eastern flank of the basin-wide near-surface clockwise circulation over the Atlantic (called the Bermuda High).

7. Atmospheric Water Cycle in the Tropics

The principal elements of the atmospheric water cycle during NH summer are displayed in Figure 7 which shows precipitation (P), evaporation (E), P–E, and vertically integrated moisture flux convergence (MFC) in July. The July P from a more observation based data set was shown earlier (Fig. 6, bottom); all fields in Figure 7, including P, are obtained from short-term forecasts of the European Center for Medium Range Weather Forecast (ECMWF) model that is constrained by meteorological observations. Evaporation is, not unexpectedly, large over ‘oceanic desert’ regions that are neither energy nor water limited. Summer evaporation is also large over midlatitude continents where precipitation is significant in the preceding seasons, especially winter. Winter and spring precipitation remains sequestered in the land-surface in these energy-limited seasons, and is released in late spring and summer when abundant solar energy is available to fuel evapotranspiration.

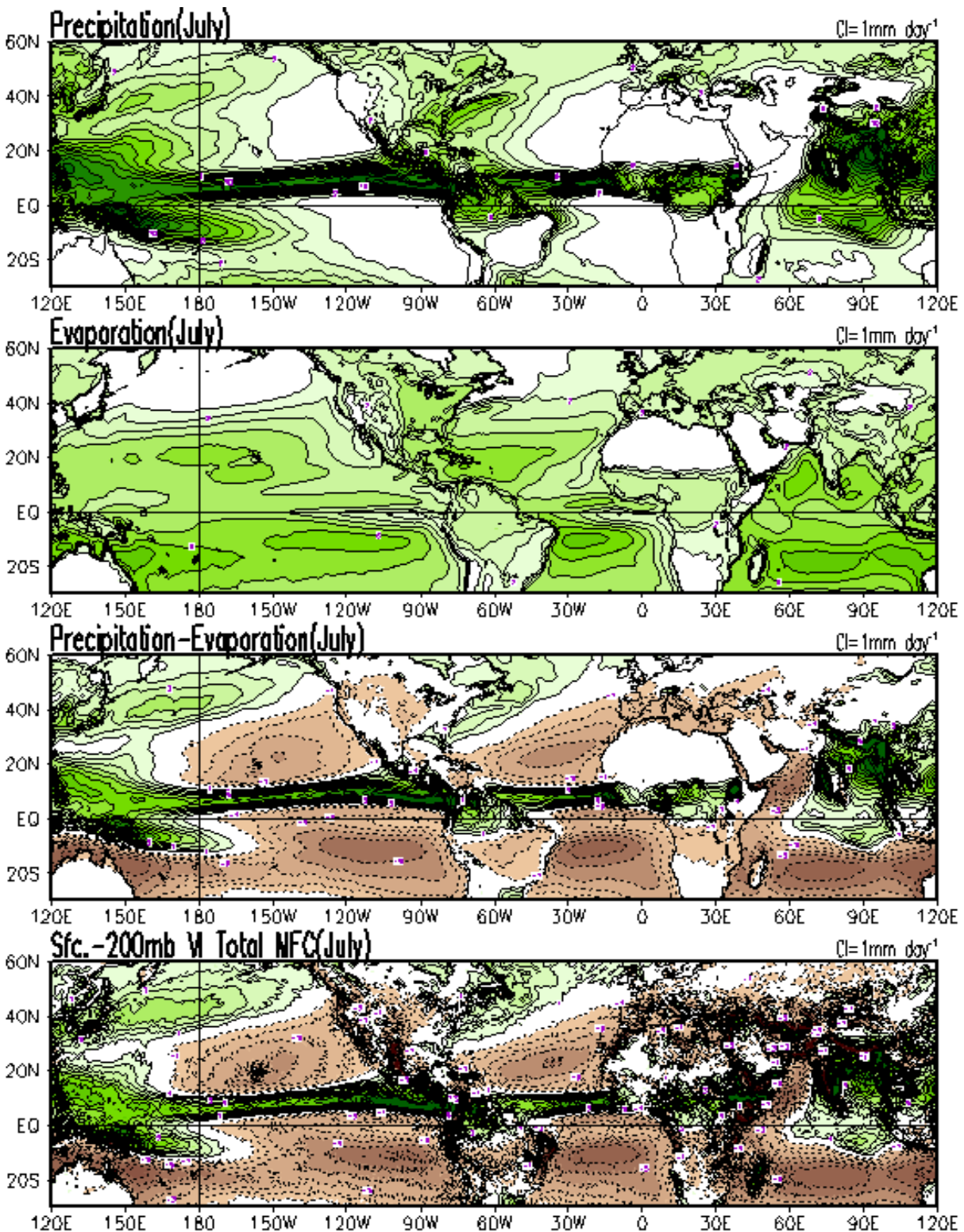


Figure 7: Climatological July precipitation (P, top), evaporation (E, second from top), precipitation minus evaporation (P-E, second from bottom), and the vertically integrated (surface to 200 hPa) moisture flux convergence (MFC, bottom). All fields are contoured with a 1.0 mm/day interval; positive (negative) values are shaded green (brown). All fields, including precipitation, are from the ERA-Interim atmospheric reanalysis (Dee et al. 2011). Climatology is based on the 1979-2014 period – the satellite-era.

The imbalance between P and E, or P–E, highlights the regions from (and to) where moisture needs to be moved. Not surprisingly, the oceanic deserts are net exporters of moisture while the ITCZ, SPCZ, and Central America are net importers, with the import generated from the low-level flow driven moisture transports.

8. Inter-Basin Salinity Differences and the Isthmus of Panama

The climatological July surface salinity is shown in Figure 8. Immediately apparent is the large salinity in the subtropics, consistent with the expansive near-surface anticyclonic circulations (Fig. 6, bottom panel) and related descending motions that generate clear skies, and thus large evaporation (Fig. 7, second from top) and salinity. Also evident are plumes of low salinity near the mouth of major rivers, e.g., the Amazon’s. The large freshwater flux from the Brahmaputra and Ganges rivers into the Bay of Bengal is reflected in the lower salinity of the northern Bay. The July salinity difference between the seas adjoining the India subcontinent is also shaped by evaporation (larger over Arabian Sea) and monsoon precipitation (larger over Bay of Bengal, cf. Fig. 7), both leading to a saltier Arabian sea. Like river discharge, regions of high precipitation are also imprinted on surface salinity, e.g., the ITCZ structure is discernible in the northern equatorial latitudes of the Pacific.

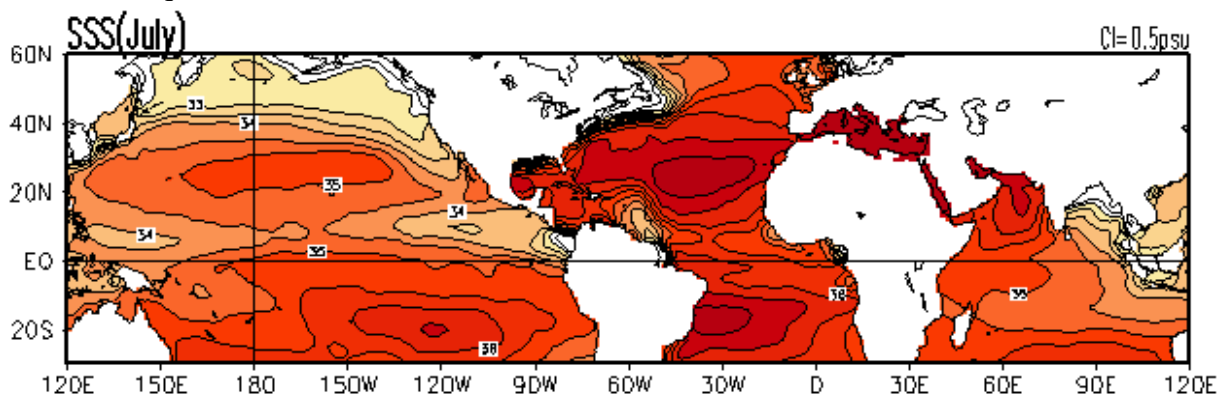


Figure 8: Climatological July sea surface salinity from the UK Met Office EN4 data set (Good, Martin, and Rayner 2013). The contour interval is 0.5 *psu*, and the climatology is for the 1979-2013 period. ‘*psu*’ is the practical salinity unit, based on seawater conductivity. 1.0 *psu* is equivalent to 1gram of salt per 1Kilogram of water, with sodium chloride and magnesium sulfate being the primary salts.

A region of strikingly low salinity in the entire tropical Pacific – the freshest waters – are, interestingly, found off the coast of Panama in northern summer (cf. Fig. 8). The fresh water tongue is apparently generated by heavy summer rainfall in the ITCZ and confined to the coastal zone by the eastward-flowing north equatorial counter current (Alory et al. 2012).

Also apparent in Figure 8 is the larger salinity of the Atlantic basin vis-à-vis the Pacific and Indian ones. The salinity difference between the Pacific and Atlantic has been attributed to the rise of the isthmus of Panama, i.e., to the closing of the Central American Seaway. The closing inhibits water (and salinity) exchange between the two basins, and thus development of common water mass properties. The rise of the isthmus about 5 million years ago led to a saltier Atlantic, from the pick-up of moisture over the tropical Atlantic (including Caribbean Seas) by the trade winds (blowing from east to west), and its subsequent release as precipitation over the eastern tropical Pacific, all as schematically shown in Figure 9 (Haug and Keigwin 2004). As there is no similar influx of water vapor at the Atlantic's eastern boundary, the Atlantic loses water while the

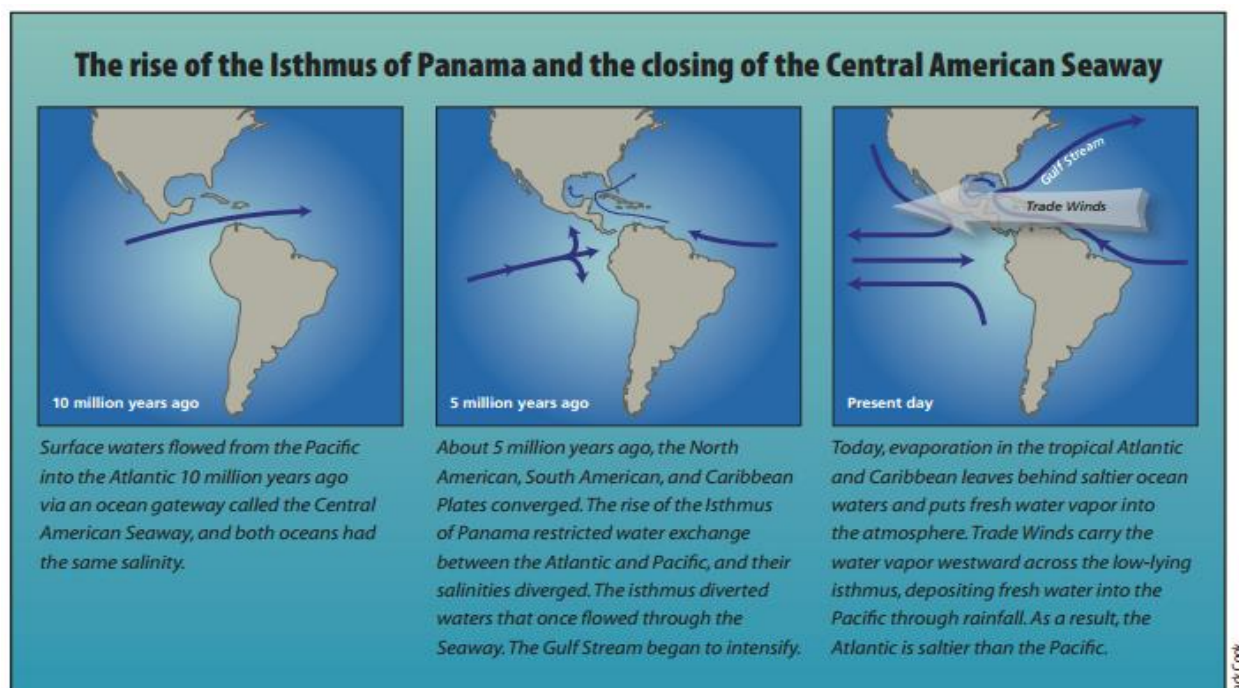


Figure 9: Inter-basin salinity differences and the Isthmus of Panama. (from Haug and Keigwin, 2004).

Pacific gains it, at least, on this account. There is no moisture influx into the Atlantic from the Indian Ocean as the intervening African continent heats up, generating continental convection and rainfall. Summer evaporation over the Indian Ocean is also effectively channeled towards peninsular India by the southwesterly winds, generating monsoon rainfall over South Asia.

9. Declining Rainfall over Gangetic Plain: Anthropogenic Change or Natural Variability?

The Indo-Gangetic Plain extending from eastern Pakistan to the Bay of Bengal is home to more than half a billion people and the agricultural heartland of South Asia. Rapid population and economic growth have led to significant land-use land-cover change (Foley et al. 2005), heightened demand for fresh water (Amarasinghe et al. 2007) and energy, degraded environment from aerosol and dust loadings (Ramaswamy et al. 2001; Seinfeld et al. 2004; Ramanathan et al. 2005), and increased greenhouse gas (GHG) emissions – all potentially influential on the summer monsoon which provides ~75% of annual rainfall over the Indian subcontinent.

The hydroclimate (e.g., precipitation, soil moisture, temperature, groundwater) of the Indo-Gangetic Plain exhibits substantial – at times, precarious – trends, especially in the post-1950s period (Naidu et al. 2009; Rodell et al. 2009). The interaction of anthropogenic factors and their feedback on climate makes attribution of regional hydroclimate variability and change challenging.

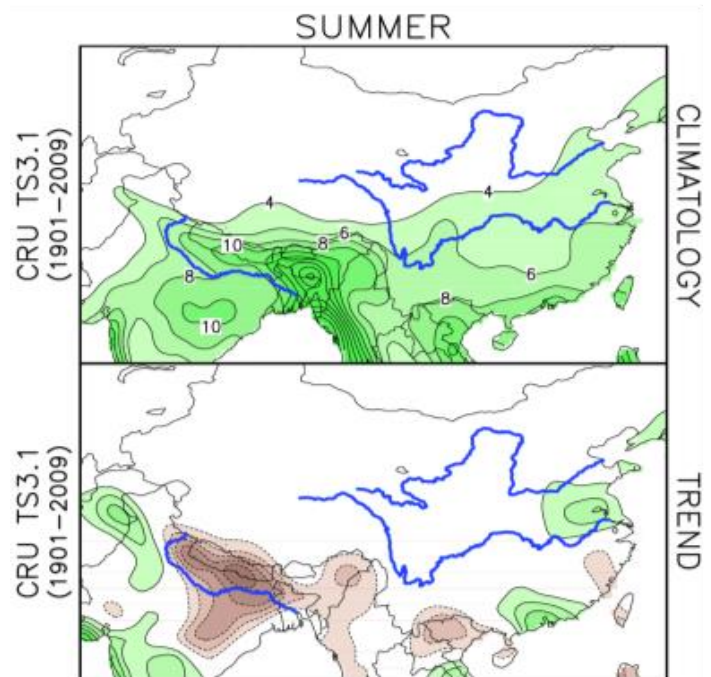


Figure 10: Climatological rainfall (CRU TS3.1, Harris et al. 2014) contoured at 2.0 mm/day (top panel; values \geq 4.0 mm/day shaded). The linear trend during 1901-2009 is plotted at 0.5 mm/day per century interval in lower panel. Yellow and Yangtze rivers in China and Ganges in India are shown in blue.

The climatological summer rainfall and its linear trend are shown in Figure 10. The declining trend is steepest (~ 1.5 mm/day per century) over the central Gangetic Plain and Himalayan foothills where rainfall is ~ 8 mm/day; the trend is thus significant as it represents $\sim 15\%$ decline in summer monsoon rainfall over the 20th century.

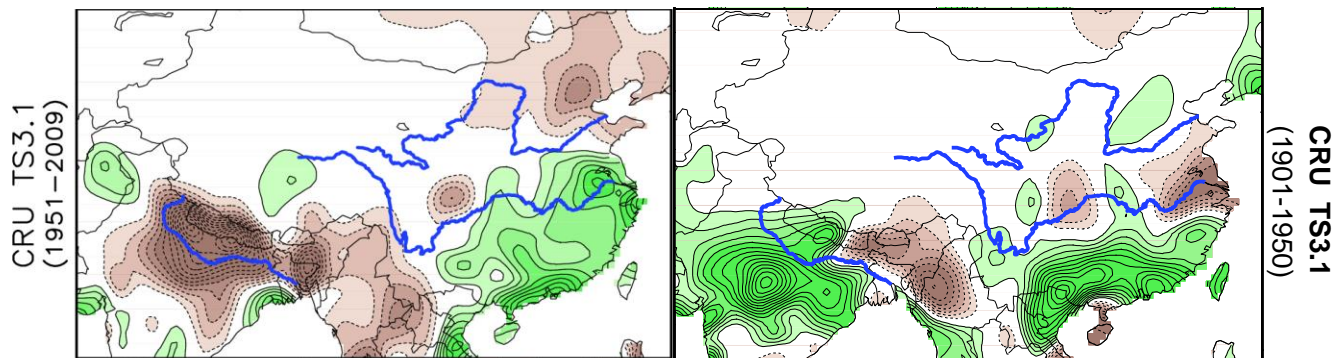


Figure 11: Linear *trend* in summer rainfall in the second (left) and first (right) half of the 20th century is plotted at 0.5 mm/day/century interval in the 0.5° latitude-longitude resolution CRU-TS3.1 surface observation dataset (University of East Anglia, Harris et al. 2014)

Multidecadal Trends: Structure

Even more significant trends (of both signs) are present in the *post-1950* period (Fig. 11, left panel): The drying trend over northern India, southeast Asia, and northeastern China, and the wetting trend over southeastern China. Rainfall trends in the *first-half* of the 20th century (1901-1950; Fig. 11, right panel) are however of **opposite** sign, both over the Gangetic Plain and eastern China (between and north of the rivers)! *Is the recent steep decline in summer monsoon rainfall over the Gangetic Plain indicative of accelerated anthropogenic effects, multidecadal natural variability (e.g., rooted in the oceans), or both?*

The opposite rainfall trends over the Gangetic Plain are often attributed to the rising GHG concentration – which increases land-ocean contrast and thus monsoon rainfall in climate models (Ueda et al. 2006; Bollasina et al. 2011; see Menon et al. 2013) – and anthropogenic aerosols (absorptive and reflective) whose loading has increased significantly in the postwar period, and

which more than offset the GHG-related increasing rainfall trend in recent decades (Ramanathan et al. 2005; Meehl et al. 2008; Bollasina et al. 2011). Interestingly, many of the cited studies are based on experiments with climate models which can simulate many aspects of the monsoon circulation but whose simulation of regional hydroclimate remains

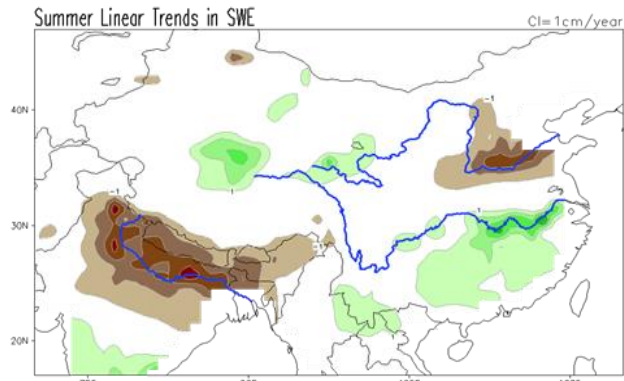


Figure 12: Summer linear trend in terrestrial water equivalent thickness during 2003-2010 from the GRACE satellite gravity solutions. Brown and green show depletion/ accumulation of ground water; contour interval is 1 cm/year.

deficient (Annamalai et al. 2007; Bollasina and Nigam 2009; Sperber et al. 2013). The models' ability to generate realistic internal variability on multidecadal time scales is furthermore limited (Deser et al. 2012; Furtado et al. 2011), precluding their use in fair appraisals of the contribution of multidecadal natural variability in the development of recent hydroclimate trends over Monsoon Asia.

The recent declining rainfall trends do find corroboration in the objectively assessed storage of groundwater from the GRACE satellite mission (Tiwari et al. 2009; Rodell et al. 2009), notwithstanding its short record. The depleting stores in Figure 12 reflect both diminished input (rainfall) and increased withdrawal (irrigation).

Multidecadal Trends: Origin

A preliminary analysis of the link between Pacific decadal SST variability and South Asian monsoon rainfall is presented to motivate the need for considering *both* decadal variability of the physical climate system and anthropogenic effects when seeking understanding (attribution) of the impressive drying of the Gangetic Plain in recent decades (Fig. 11, left panel), following

Nigam et al. (2015). In this analysis *SST is the fulcrum*: Its multidecadal natural variability and secular trend are used to parse the rainfall record into similar components via linear regression.

The multidecadal natural variability and secular change components of SST variability are simultaneously characterized using the extended-empirical orthogonal function (E-EOF) analysis (Guan and Nigam 2008), i.e., contextually, as opposed to residual estimation of the natural variability component. The analysis is able to discriminate between El Niño Southern Oscillation (ENSO), Pacific decadal variability, and the *nonstationary* SST Secular Trend, all without any advance filtering and potential aliasing of the SST record. The principal component (PC) representing North Pacific decadal SST variability in this analysis (PDV-NP) closely tracks the Pacific Decadal Oscillation index (PDO, Mantua et al. 1997).

The North Pacific decadal SST variability exhibits significant links to Asian summer monsoon rainfall (Fig. 13): The negative anomaly over Gangetic Plain and the meridional dipole over eastern China, structurally, resemble the post-1950 rainfall trends (Fig. 11, left panel)! Although PDO's link with monsoon

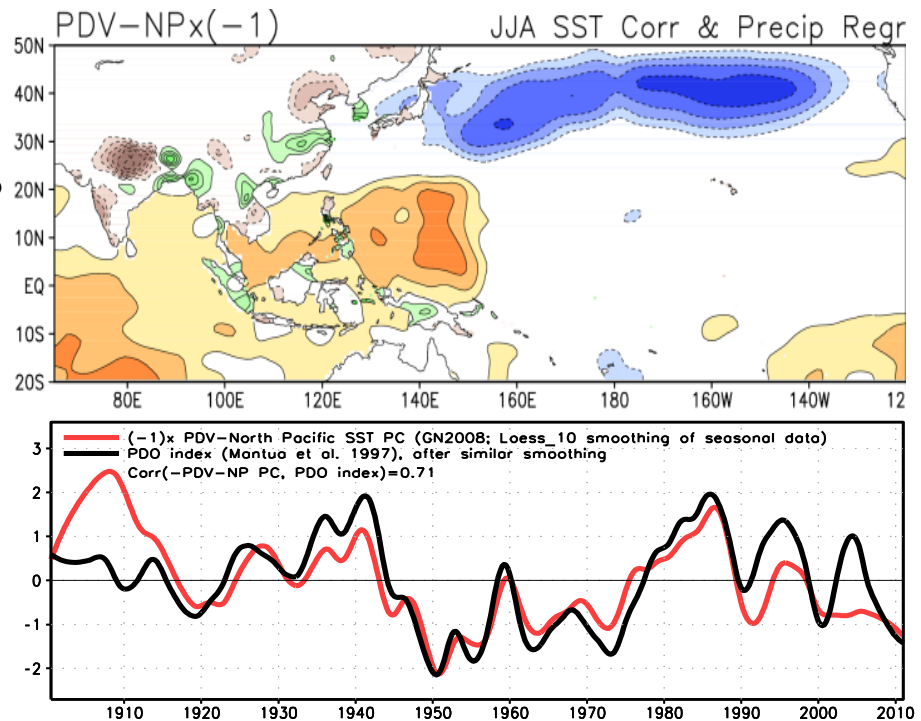


Figure 13: Principal component (PC) of North Pacific decadal SST variability $\times (-1)$ in red, along with Mantua's PDO index (in black). Linear regressions of the PC on continental summer rainfall are shown in brown/green with an interval of 0.1 mm/day. Linear correlations with SSTs are shown in blue/red with an interval of 0.1; both analyses for the 1901-2009 period.

rainfall was noted almost a decade ago, it has not been exploited in advancing the understanding, modeling, and prediction of decadal rainfall variations because articulation of the underlying mechanisms has been challenging – in view of the widely noted midlatitude focus of the PDO SSTs and the prevailing paradigm where only tropical SST anomalies are deemed influential.

Guan and Nigam (2008) showed – perhaps, for the first time – the striking links of the PDV-NP (or PDO) to the Indo-Pacific warm pool SSTs, from correlation analysis. The revelation of PDV-NP's tropical SST links suggests that its influence on Asian monsoon rainfall could be grounded in more than statistics. The PDV-NP's tropical SST links open the door to a vast, mature body of research on influence mechanisms, while its Indian basin links allow tapping into the monsoon paradigm. For example, the Gangetic Plain rainfall decline is in accord with the basic notion on monsoon origin – land-ocean contrast – which would be less for a warmer Indian Ocean.

The analysis is cautionary: It cautions against readily attributing multidecadal hydroclimate trends to anthropogenic effects. Multidecadal natural variability of the climate system – for example, as manifest in Pacific and Atlantic basin surface and sub-surface temperatures, and related influence – must be factored for in any meaningful attribution. The anthropogenic signal obtained in this manner should be more robust, and at times, even more pronounced than the routine linear trend.

References

- Adler, R.F., and Coauthors, 2003: The Version 2 Global Precipitation Climatology Project (GPCP) Monthly Precipitation Analysis (1979-Present). *J. Hydrometeor.*, **4**, 1147-1167.
- Alory, G., C. Maes, T. Delcroix, N. Reul, and S. Illig, 2012: Seasonal dynamics of sea surface salinity off Panama: The far Eastern Pacific Fresh Pool. *J. Geophys. Res.*, **117**, C04028, doi:[10.1029/2011JC007802](https://doi.org/10.1029/2011JC007802).
- Amarasinghe, U. A., T. Shah, and O. P. Singh, 2007: Changing consumption patterns: Implications on food and water demand in India. Colombo, Sri Lanka: International Water Management Institute (IWMI) 37p. *IWMI Research Report 119*. doi: 10.3910/2009.119.
- Annamalai, H., K. Hamilton, and K. Sperber, 2007: The South Asian summer monsoon and its relationship with ENSO in the IPCC AR4 simulations. *Journal of Climate*, **20**, 1071-1092.
- Bollasina, M., Y. Ming, and V. Ramaswamy, 2011: Anthropogenic Aerosols and the Weakening of the South Asian Summer Monsoon. *Science*, **334**, 502-505.
- Bollasina, M., and S. Nigam, 2009a: Indian Ocean SST, evaporation, and precipitation during the South Asian summer monsoon in IPCC-AR4 coupled simulations. *Climate Dynamics*, **33**, 1017-1032.
- Dee, D. P., and Coauthors, 2011: The ERA-Interim reanalysis: configuration and performance of the data assimilation system. *Q.J.R. Meteorol. Soc.*, **137**: 553–597. doi: 10.1002/qj.828.
- Deser, C., and Coauthors, 2012: ENSO and Pacific Decadal Variability in the Community Climate System Model Version 4. *Journal of Climate*, **25**, 2622-2651.
- Foley, J., and Coauthors, 2005: Global consequences of land use. *Science*, **309**, 570-574.
- Furtado, J., E. Di Lorenzo, N. Schneider, and N. Bond, 2011: North Pacific Decadal Variability and Climate Change in the IPCC AR4 Models. *Journal of Climate*, **24**, 3049-3067.
- Good, S. A., M. J. Martin and N. A. Rayner, 2013: EN4: Quality controlled ocean temperature and salinity profiles and monthly objective analyses with uncertainty estimates. *Journal of Geophysical Research: Oceans*, **118**, 6704-6716, doi:[10.1002/2013JC009067](https://doi.org/10.1002/2013JC009067).
- Guan, B., and S. Nigam, 2008: Pacific sea surface temperatures in the twentieth century: An evolution-centric analysis of variability and trend. *Journal of Climate*, **21**, 2790-2809.

- Harris, I., Jones, P.D., Osborn, T.J. and Lister, D.H., 2014: Updated high-resolution grids of monthly climatic observations – the CRU TS3.10 Dataset. *Int. J. Climatol.*, 34: 623–642. doi:10.1002/joc.3711
- Haug, G. H., and L. D. Keigwin, 2004: [How the Isthmus of Panama Put Ice in the Arctic?](#) *Oceanus*, Vol. 42, No. 2, April.
- Kalnay, E., and Coauthors, 1996: The NCEP/NCAR 40-Year Reanalysis Project. *Bull. Amer. Meteor. Soc.*, 77, 437–471.
- Mantua, N., S. Hare, Y. Zhang, J. Wallace, and R. Francis, 1997: A Pacific interdecadal climate oscillation with impacts on salmon production. *Bulletin of the American Meteorological Society*, **78**, 1069-1079.
- Meehl, G., J. Arblaster, and W. Collins, 2008: Effects of black carbon aerosols on the Indian monsoon. *Journal of Climate*, **21**, 2869-2882.
- Menon, A., A. Levermann, J. Schewe, J. Lehmann, and K. Frieler, 2013: Consistent increase in Indian monsoon rainfall and its variability across CMIP-5 models. *Earth System Dynamics*, **4**, 287-300.
- Mitchell, T.P, and J.M. Wallace, 1992: The Annual Cycle in Equatorial Convection and Sea Surface Temperature, *J. Climate*, **5**, 1140-1156.
- Munoz, E., A. J. Busalacchi, S. Nigam, and A. Ruiz-Barradas, 2008: [Winter and summer structure of the Caribbean Low-Level Jet](#). *J. Climate*, 21, 1260-1276.
- Naidu, C., K. Durgalakshmi, K. Krishna, S. Rao, G. Satyanarayana, P. Lakshminarayana, and L. Rao, 2009: Is summer monsoon rainfall decreasing over India in the global warming era? *Journal of Geophysical Research-Atmospheres*, **114**.
- Nigam, S., Y. Zhao, A. Ruiz-Barradas, and T. Zhou, 2015: The South-Flood North-Drought Pattern over Eastern China and the Drying of the Gangetic Plain: Observations, Simulations, and Origin. Invited book chapter (pgs. 347-360) in *Climate Change: Multidecadal and Beyond* (Editors: Michael Ghil, Mojib Latif, Mike Wallace and C.P. Chang) World Press, 376p.
- Nigam, S. and Y. Chao, 1996: Evolution Dynamics of Tropical Ocean-Atmosphere Annual Cycle Variability, *J. Climate*, **9**, 3187-3205.
- Philander, S.G.H. and Y. Chao, 1991: On the Contrast between the Seasonal Cycles of the Equatorial Atlantic and Pacific Oceans, *J. Phys. Oceanogr.*, **21**, 1399-1406.

- Ramanathan, V., and Coauthors, 2005: Atmospheric brown clouds: Impacts on South Asian climate and hydrological cycle. *Proceedings of the National Academy of Sciences of the United States of America*, **102**, 5326-5333.
- Ramaswamy, V., O. Boucher, J. Haigh, D. Hauglustane, J. Haywood, G. Myhre, T. Nakajima, G. Y. Shi, and S. Solomon (2001), Radiative forcing of climate change, in *Climate Change 2001: The Scientific Basis*, Chap. 6, edited by J. T. Houghton et al., pp. 349–416, Cambridge Univ. Press, Cambridge.
- Rayner, N. A., D. E. Parker, E. B. Horton, C. K. Folland, L. V. Alexander, D. P. Rowell, E. C. Kent, and A. Kaplan, 2003: Global analyses of sea surface temperature, sea ice, and night marine air temperature since the late nineteenth century, *J. Geophys. Res.*, 108(D14), 4407, doi:10.1029/2002JD002670.
- Rodell, M., I. Velicogna, and J. Famiglietti, 2009: Satellite-based estimates of groundwater depletion in India. *Nature*, **460**, 999-U980.
- Seinfeld, J., and Coauthors, 2004: ACE-ASIA - Regional climatic and atmospheric chemical effects of Asian dust and pollution. *Bulletin of the American Meteorological Society*, **85**, 367.
- Sperber, K., and Coauthors, 2013: The Asian summer monsoon: an intercomparison of CMIP5 vs. CMIP3 simulations of the late 20th century. *Climate Dynamics*, **41**, 2711-2744.
- Tiwari, V., J. Wahr, and S. Swenson, 2009: Dwindling groundwater resources in northern India, from satellite gravity observations. *Geophysical Research Letters*, **36**.
- Ueda, H., A. Iwai, K. Kuwako, and M. Hori, 2006: Impact of anthropogenic forcing on the Asian summer monsoon as simulated by eight GCMs. *Geophysical Research Letters*, **33**.
- Weaver, S.J., and S. Nigam, 2008: [Variability of the Great Plains Low-Level Jet: Large-scale circulation context and hydroclimate impacts](#). *J. Climate*, 20, 1532-1551.